A method for deriving displacement data during cyclical movement using an inertial sensor

Thilo Pfau[1,*], Thomas H. Witte[1] and Alan M. Wilson[1,2]

[1]*Structure and Motion Laboratory, The Royal Veterinary College, Hawkshead Lane, Hatfield, Hertfordshire, AL9 7TA, UK* and [2]*Structure and Motion Laboratory, Royal National Orthopaedic Hospital, Brockley Hill, Stanmore, Middlesex, HA7 4LP, UK*

*Author for correspondence (e-mail: tpfau@rvc.ac.uk)

Summary

Biomechanical studies often employ optical motion capture systems for the determination of the position of an object in a room-based coordinate system. This is not ideal for many types of study in locomotion since only a few strides may be collected per 'trial', and outdoor experiments are difficult with some systems. Here, we report and evaluate a novel approach that enables the user to determine linear displacements of a proprietary orientation sensor during cyclical movement. This makes experiments outside the constraints of the laboratory possible, for example to measure mechanical energy fluctuations of the centre of mass during over-ground locomotion. Commercial orientation sensors based on inertial sensing are small and lightweight and provide a theoretical framework for determining position from acceleration. In practice, the integration process is difficult to implement because of integration errors, integration constants and the necessity to determine the orientation of the measured accelerations. Here, by working within the constraints of cyclical movements, we report and evaluate a method for determining orientation and relative position using a modified version of a commercial inertial orientation sensor that combines accelerometers, gyroscopes and magnetometers, thus giving a full set of movement parameters (displacement, velocity and acceleration in three dimensions). The 35 g sensor was attached over the spine of a horse exercising on a treadmill. During canter locomotion (9.0 m s^{-1}), the amplitudes of trunk movement in the x (craniocaudal), y (mediolateral) and z (dorsoventral) directions were 99.6, 57.9 and 140.2 mm, respectively. Comparing sensor displacement values with optical motion capture values for individual strides, the sensor had a median error (25th, 75th percentile) in the x, y and z directions of 0.1 (–9.7, +10.8), –3.8 (–15.5, +13.7) and –0.1 (–6.3, +7.1) mm, respectively. High-pass filtering of the displacement data effectively separated non-cyclical from cyclical components of the movement and reduced the interquartile ranges of the errors considerably to (–3.6, 6.2), (–4.0, 3.8) and (–4.5, 5.1) for x, y and z displacement, respectively, during canter locomotion. This corresponds to (–3.2, 5.5)%, (–6.7, 6.3)% and (–3.3, 3.7)% of the range of motion.

Key words: inertial sensor, accelerometer, motion analysis, gait, horse, kinematics.

Introduction

Biomechanical studies traditionally employ optical motion capture systems for the determination of the position of an object in a room-based coordinate system. This constrains experiments to the calibrated volume of the camera system (although the cameras may move). This is not ideal for many types of study in locomotion since only a few strides may be collected per 'trial', and outdoor experiments are difficult with some systems. This is especially problematic where maximal activity is involved or the subjects have limited exercise capacity. Whilst treadmills are often used to provide a solution, these are not ideal or feasible under all circumstances. It is also difficult to study stride-to-stride variability in movement, generate the large data sets required for processing using statistical pattern recognition techniques or investigate locomotion involving different surfaces, inclines and obstacles. Here, we report and evaluate a novel approach that enables the user to determine linear displacements of a proprietary orientation sensor during cyclical movement. This makes it possible to undertake some of the experiments outlined above outside the constraints of the laboratory. Examples of such experiments include mechanical energy fluctuations of the centre of mass, horse rider interaction, interaction of athletes with their equipment (for instance, racing cyclists) and stride kinematics in subjects with prosthetic limbs, high susceptibility to falling and in different environments (surface, obstacles, light levels).

One important application of this approach is the quantification of external work. External work, the work that

an individual performs against the environment that results in changes in the potential energy (E_p) and kinetic energy (E_k) of the centre of mass (CoM), represents a major component of the mechanical work of locomotion (Cavagna, 1975) and is often evaluated as a measure of locomotor efficiency on different surfaces (Ferris et al., 1998), in locomotion with prosthetic limbs (Skinner and Effeney, 1985; Tesio et al., 1998) or to justify gait choice (Minetti et al., 1999). Vertical displacements and velocities in three dimensions are needed to calculate changes in E_p and E_k. External work is traditionally calculated either from force plate data or by summing individual body segment E_k and E_p. Both are time-consuming approaches; the former requires a force plate and knowledge of initial conditions, and the latter requires a large set of marker coordinates and knowledge of segmental inertial properties (Buchner et al., 2000; Minetti et al., 1999). These analyses are therefore rarely undertaken and are usually confined to treadmill locomotion or low-speed locomotion over a force platform. Since the influences on external work of factors such as incline, surface stiffness and gait are of interest, this represents a major limitation. Another disadvantage is the differences between treadmill and over-ground locomotion that have been reported for both horses and humans (Elliott and Blanksby, 1976; Nigg et al., 1995). In the horse, when compared to over-ground locomotion, treadmill locomotion displays several key mechanical differences including reduced vertical trunk displacement and increased stride length (Barrey et al., 1993; Buchner et al., 1994b).

A good estimate of CoM displacement and velocity can be gained from overall trunk movement since limb movement is out of phase in the majority of bipedal and quadrupedal gaits and changes of potential energy of the limbs are small (data from Wilson et al., 2003). This is especially true for cursorial animals due to their relatively low limb mass (e.g. 5.8% and 5.5% of the total body mass for the hind limbs and forelimbs of the horse, respectively; Buchner et al., 1997). Although limb, head and visceral movements cause the CoM to change location within the trunk, visceral movements can only be quantified by the use of force platforms as ergometers (Cavagna, 1975). If head movement is considered an important factor for CoM movement, it can easily be captured by an additional marker (in case of optical motion capture) or an additional sensor (this approach) and included in the calculations of the CoM. However, if the CoM can be considered to lie in a fixed position, then the six degree of freedom (DoF) movement of that position can be determined either from the movement of at least three markers in three dimensions or the six DoF position of a single point that lies a known distance and orientation from the assumed CoM. This simplifies the measurement procedure; however, motion analysis data are still required.

Here, we are interested in examining movement outside the laboratory when collection of motion capture or force plate data is not feasible. The approach is to integrate acceleration data to determine position. Through the advent of low-cost, miniature triaxial accelerometers, direct measurement of acceleration has become feasible. However, the process of determining velocity and position by integration from acceleration is more problematic than the reverse. Errors rapidly accumulate during the integration process and additional knowledge in the form of initial conditions is required for determination of integration constants. Attempts to track motion by integration of accelerometer signals are therefore often unsuccessful unless low-pass filtering is permitted at each integration or very high quality, expensive and bulky equipment is used (Barrey et al., 2001; Barrey and Galloux, 1997; Leleu et al., 2002). The technique is therefore usually the preserve of military engineering.

In the integration process, changes in accelerometer orientation must be accounted for since an accelerometer measures acceleration relative to its orientation rather than to the earth or global coordinate system. This underlies the application of accelerometers as inclinometers in electronic spirit levels, where they determine the component of gravity that acts orthogonal to the level. Accelerometer orientation has previously been determined in two ways; by optical motion capture systems (Hedrick et al., 2004), which encounter the inherent problems discussed above, and by angular rate gyroscopes. The angular velocity output of a gyroscope can be integrated to determine orientation, so three orthogonal gyroscopes can be used to sense the orientation of a triaxial accelerometer. Again, integration errors will accumulate over time, resulting in drift, and knowledge of initial orientation is required. One solution is to use the known orientation of the earth's gravitational field, but this becomes difficult during movement and does not enable correction for the integration errors. It also does not allow for correction of heading. Alternatively, it is possible to obtain an absolute measure of orientation using the earth's magnetic field, as in a compass, which uses the horizontal components for heading determination. The earth's magnetic field also has a vertical component (hence why an un-weighted compass needle will dip), and a triaxial magnetometer can therefore sense absolute two-dimensional (2D) orientation, since it is not possible to sense rotations about the axis of the earth's magnetic field. A combination of accelerometers and magnetometers will therefore give absolute three-dimensional (3D) orientation, except at the magnetic North and South pole (where gravity and earth magnetic field are parallel).

Sub-miniature accelerometers, gyroscopes and magnetometers, with a mass of 1 g or less and costing as little as $10, are readily available. These MEMS (micro-electro-mechanical systems) accelerometers contain silicon beams, which deform during acceleration. Resultant changes in capacitance are processed within the chip, which outputs a voltage relative to the applied acceleration. Miniature gyroscopes that sense Coriolis forces when rotations are applied to a pair of oscillating tines have been developed for applications such as movement compensation in hand-held video cameras, and small magnetometers are widely employed in electronic compasses.

Several companies have developed inertial sensors

combining all three technologies, which give orientation in a global coordinate system (relative to the earth's magnetic and gravitational fields). These are used in a wide array of applications, such as virtual reality systems, where they sense the orientation of the head mounted display of the subject. Since they give orientation information and can sense 3D acceleration, these transducers provide the basis for determining position by integration of acceleration. However, as alluded to above, the integration process from acceleration to velocity and displacement remains challenging. Here, we focus on the implementation of an appropriate integration procedure that, in combination with the available orientation estimates, allows us to track movements with six DoF. This process would allow the application of miniature inertial sensors for an enormous range of animal tracking and locomotion studies, making studies of real-life activities under non-laboratory conditions possible.

The approach proposed is based on the cyclical nature of locomotion. This means that it is possible to mean subtract the data, effectively meaning that the sensor path is constrained to return to its starting point over a cycle. The period used for mean subtraction will represent a trade-off between minimising the accumulation of integration errors and capturing features that extend over a longer period of time (for instance, tripping and jumping).

For example, during steady-state, level locomotion it is reasonable to assume that changes in the E_k and E_p of the trunk between strides are either small or zero. This means that trunk displacement data should follow a closed loop (subtracting the effect of forward motion). The average velocity over the stride (or several strides) should be zero, and the average forward–backward and side-to-side acceleration should be zero. Furthermore, the measured average vertical acceleration should equal g (the gravitational constant). Thus, stride-by-stride mean subtraction of acceleration and of the calculated velocity vectors before integration theoretically enables determination of the integration constants. Applying mean subtraction over individual strides constrains the movement pattern to steady-state, level locomotion. However, relaxing the mean subtraction to a series of strides (a standard technique for dealing with data drift) enables evaluation of inter-stride variability with the cost of greater accumulation of integration errors.

Here, we develop an approach for deriving displacement data from a commercial orientation sensor by integration and mean subtraction. The results and errors of our approach are compared to the 'gold standard' of 3D optical motion analysis.

Materials and methods

Initial experiments with inertial tracking were undertaken with a 2D sensor manufactured in-house using two accelerometers and one gyroscope. However, ensuring that the individual components were mounted exactly orthogonal to each other proved difficult and we moved to using a commercially available orientation sensor with a modified sensor bandwidth (MT9; Xsens, Enschede, The Netherlands). This unit contained the nine sensors required, a temperature sensor (to correct for temperature drift), low-pass filter circuits and a microcontroller, which digitized the data and combined the 10 data streams into a single serial data stream. These sensors are designed for determining orientation but were suitable for our application once the bandwidth was changed. The sensor fusion algorithm (Xsens) used accelerometer and magnetometer data (at times of slow movements of the sensor) to sense gravity and magnetic North and to compensate for otherwise unlimited increasing errors from the integration of rate of turn data. The sensor contained accelerometers with a dynamic range of $\pm 10\,g$ and gyroscopes with a range of ± 900 deg. s^{-1}. Maximum accelerations measured in the experiments were obtained at high-speed canter and were in the region of $5\,g$. Peak angular velocities were in the range of 250 deg. s^{-1}. All the sensors have a rapid response time, and data were low-pass filtered in order to reduce measurement noise. In our modified sensor, accelerometer and gyroscope low-pass filter cut-off frequencies (6 dB per octave Butterworth filter) were adapted from 30 Hz to 50 Hz for accelerometer and gyroscope data, and magnetometer data were low-pass filtered at 10 Hz (as a comparison, a minimum stance time of ~80 ms, corresponding to a frequency of ~12.5 Hz in horizontal acceleration and 6.25 Hz in vertical acceleration, can be observed for Thoroughbred race horses at racing speed). All data were then passed through a 14-bit AD converter. Each sensor was sampled 250 times per second. The output was an RS232 (serial) data stream at 115 200 bit s^{-1}.

Three experiments were undertaken:

(1) confirmation of accuracy of optical motion capture system;

(2) accuracy of MT9 inertial sensor determined by direct comparison to optical motion capture;

(3) measurement of trunk movement of a Thoroughbred horse during treadmill locomotion.

Experiment 1 – accuracy of optical motion capture system

The accuracy of the optical motion capture system under our experimental conditions was determined by attaching two spherical retro-reflective markers (diameter 30 mm) to the turntable of a record player, which was then spun at 33 and 45 r.p.m. in the field of view of the two-camera 3D motion capture system (MCU240; ProReflex, Qualisys Ltd, Gothenburg, Sweden).

The accuracy of the motion capture system was tested based on the circularity of the path of the spherical markers on the turntable of the record player. A least-mean-square error-based gradient descent method was used to find the best match of the 3D marker positions to a circle in 3D space (Barker, 2004).

Experiment 2 – accuracy of MT9 inertial sensor compared with optical motion capture determined during treadmill locomotion

Whilst not the envisaged application, treadmill locomotion is used to enable validation of many consecutive strides in a

short period of time. An MT9 inertial sensor was mounted in a custom-made harness constructed of malleable casting material (Dynacast, Smith and Nephew, Wound Management, Hull, UK) over the 4th thoracic vertebra (the withers) of a Thoroughbred horse (Fig. 1). A cable ran from the sensor, *via* an overhanging beam, to a laptop computer and battery located beside the treadmill. Serial data were collected from the sensor *via* custom software written in Microsoft Visual C++ (Microsoft Corporation, Redmond, WA, USA) using the sensor's software development kit (SDK; Xsens). A wand with three orthogonal arms, each bearing a retro-reflective spherical motion capture marker, was fixed to the sensor (Fig. 2). The positions of these markers were recorded at 240 Hz using the 3D optical motion capture system validated in experiment 1. The cameras were positioned 3 m to the left of the treadmill. The calibrated volume of the cameras was comparable to the calibrated volume used in experiment 1. A treadmill-centred right-handed Cartesian coordinate system (global system) was defined with the following conventions: the positive *x*-axis was pointing towards the front of the treadmill, the positive *y*-axis was pointing towards the left side of the treadmill and the positive *z*-axis was pointing upwards. These directions correspond to craniocaudal, mediolateral and dorsoventral movements of the withers of the horse. Three DoF tracking of the three real markers was performed using QTrac software (Qualisys Ltd) in the treadmill-centred system. Based on the positions of these three markers, six DoF tracking of one virtual marker located at the centre of the inertial sensor was carried out using custom software in MATLAB (The Mathworks Inc., Natick, MA, USA).

The beginning of each stride was determined by measuring left fore foot acceleration using a solid-state capacitive accelerometer with a dynamic range of ±50 *g* (ADXL150; Analog devices, Norwood, MA, USA; sensitivity 38 mV g^{-1}). It was protected by enclosure in epoxy-impregnated Kevlar fibres (total mass 2 g) and mounted in the dorsal midline of the hoof with the sensitive axis orientated in a proximo-distal direction (Witte et al., 2004). Output signals were telemetered *via* a narrow-band analogue FM radio telemetry device operating at 458 MHz with an audio response of 9 Hz to 3 kHz at –3 dB (ST/SR500; Wood and Douglas Ltd, Baughurst, Hampshire, UK). Data were logged at a sample rate of 1000 Hz *via* a 12-bit AD converter on a PCMCIA card (DAQcard700; National Instruments, Austin, TX, USA) into a laptop computer running custom software in MATLAB. The telemetry transmitter and battery were mounted within an elastic exercise bandage on the lateral aspect of the third metacarpal bone of the left fore limb. The mass of the telemetry unit and battery adds up to 140 g, which, together with the exercise boot, gives a total of 310 g (<1% total limb mass), a moderate additional mass in comparison with the mass of the leg. A short cable running along the lateral aspect of the digit linked the telemetry unit to the accelerometer.

The horse was habituated to the high-speed treadmill (Sato, Upsala, Sweden) before the start of the study (Buchner et al., 1994a). After a warm-up period, the horse was exercised at increments of speed between 1.4 m s^{-1} and 9.0 m s^{-1}. At each speed increment, the horse was allowed to settle into a regular gait prior to simultaneous collection of 15 s of inertial sensor, optical motion capture and accelerometer data. After discarding the first 5 s of data to allow for initializing effects of the inertial sensing to settle, this allowed us to capture a sequence of strides at each gait (walk, trot and canter).

Audio transcription software (Transcriber; http://www.etca.fr/CTA/gip/Projets/Transcriber/) was used to identify the times of foot-on from the accelerometer voltage output. A mean absolute error of 2 ms for foot-on has been determined for this system (Witte et al., 2004). Inertial sensor and optical motion capture data were processed using custom software written in MATLAB.

The position of a virtual marker created at the centre of the inertial sensor using the positions of the three optical motion capture markers was used to compare the optical motion capture data with inertial sensor data. The results were subdivided into the accuracy of orientation determination and the accuracy of measurement of linear displacements.
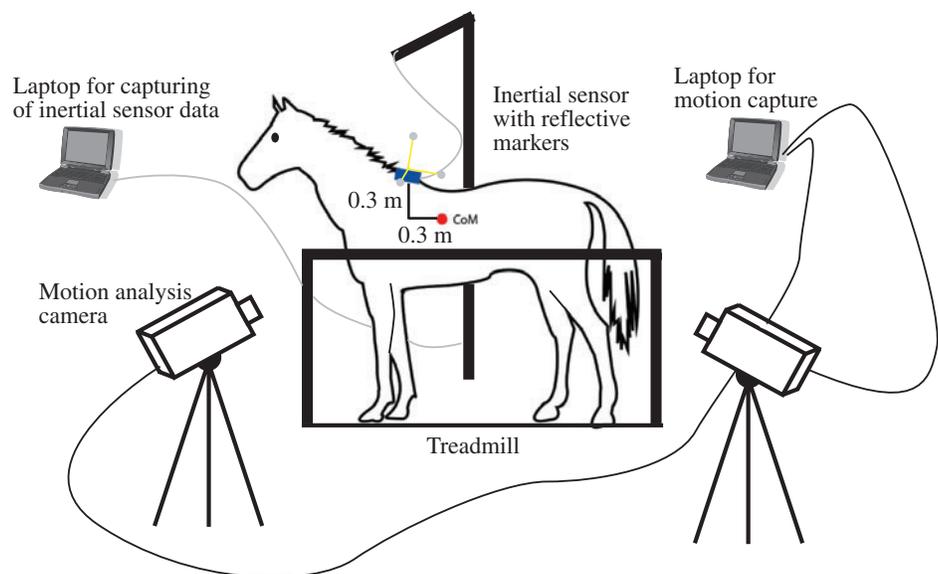

Fig. 1. Schematic drawing of the data collection set-up. The inertial sensor is mounted over the thoracic spinous processes (the withers) of the horse with the motion analysis marker wand attached. Cables are run from the inertial sensor to a laptop computer (*via* the safety harness mast) as well as from the optical motion capture cameras to a second laptop computer.

Fig. 2. The harness employed for attachment of the inertial sensor to the thoracic spinous processes of the subject animal. The wands and markers for 3D optical motion capture are also shown.

Orientation

First, we were interested in the accuracy of the inertial sensor for measurement of absolute orientation. Errors in absolute orientation will propagate into the integration process from acceleration to velocity and displacement since sensor accelerations have to be projected into the global coordinate system based on absolute orientation derived from the sensor. However, small absolute errors in orientation will have a minimal effect on the projection of the acceleration values.

The orientation algorithm of the inertial sensor provided orientation data in the earth reference frame in the form of Euler angles, quaternions or rotation matrices. Euler angles were used for the purposes of graphical display, whilst data processing was carried out using rotation matrices, which do not suffer the problem of gimbal lock. Euler angles (roll, pitch and heading) represent rotations from the sensor system into the earth reference system (horizontal and magnetic North; Fig. 3). The conventions used set the order of rotations to roll first (rotation around the sensor x-axis), then pitch (rotation around the sensor y-axis) and then heading (rotation around the sensor and then also the earth reference z-axis).

It was necessary to align the earth reference system (used to express inertial sensor orientation) with the optical motion capture reference system (global system) (Fig. 3). Therefore, initial values for roll ($r_{MT9,0}$), pitch ($p_{MT9,0}$) and heading ($h_{MT9,0}$) were recorded from the inertial sensor, while the inertial sensor was aligned with the optical motion capture coordinate system. Mean values across six positions around the expected

position on the horse were used. Inertial sensor Euler angles (r_{MT9}, p_{MT9}, h_{MT9}) were aligned to the optical motion capture coordinate system using the following equation:

$$\mathbf{euler}_{MT9,aligned}(t) = \begin{pmatrix} r_{MT9,aligned}(t) \\ p_{MT9,aligned}(t) \\ h_{MT9,aligned}(t) \end{pmatrix} = \begin{pmatrix} r_{MT9}(t) \\ p_{MT9}(t) \\ h_{MT9}(t) \end{pmatrix} - \begin{pmatrix} r_{MT9,0} \\ p_{MT9,0} \\ h_{MT9,0} \end{pmatrix}. \quad (1)$$

Subsequently, a rotation matrix, $\mathbf{R}_{sg}$, representing a rotation from the sensor system into the motion capture system (global system) was derived using the following equation, with Euler angles obtained from Eqn 1 (subscripts and time dependencies have been omitted on the right-hand side of the equation in order to improve readability):

$$\mathbf{R}_{sg}(t) = \begin{bmatrix} \cos p \cos h & \cos p \sin h & -\sin p \\ (\sin r \sin p \cos h - \cos r \sin h) & (\sin r \sin p \sin h + \cos r \cos h) & \sin r \cos p \\ (\cos r \sin p \cos h + \sin r \sin h) & (\cos r \sin p \sin h - \sin r \cos h) & \cos r \cos p \end{bmatrix}. \quad (2)$$

In addition, minor misalignment between the motion analysis marker wand and the inertial sensor was corrected for. A correction vector was determined from values of roll, pitch and heading for both methods recorded simultaneously while the inertial sensor was mounted in the harness equipped with the optical motion capture wand. Euler angles of the optical
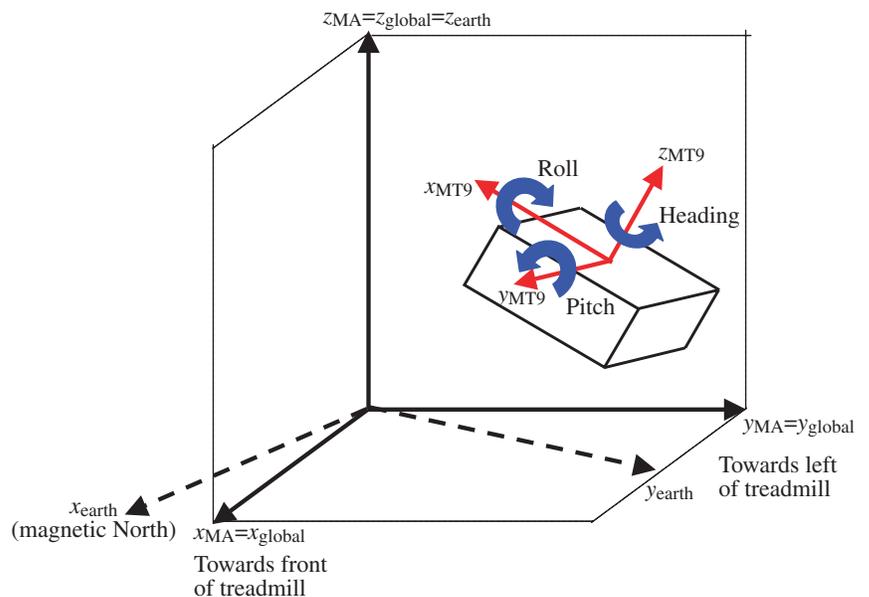

Fig. 3. Schematic drawing of the coordinate systems used. Orientation of the inertial sensor is expressed as a sequence of roll, pitch and heading from the 'sensor' into the 'earth' system. In order to compare optical motion capture and inertial sensor output, the 'global' coordinate system is used.

motion capture system were then corrected using the following equation:

$$\mathbf{euler}_{MA}(t) = \begin{pmatrix} r_{MA,aligned}(t) \\ p_{MA,aligned}(t) \\ h_{MA,aligned}(t) \end{pmatrix} = \begin{pmatrix} r_{MA}(t) \\ p_{MA}(t) \\ h_{MA}(t) \end{pmatrix} -$$

$$\left\{ \begin{pmatrix} r_{MA,harness} \\ p_{MA,harness} \\ h_{MA,harness} \end{pmatrix} - \left[\begin{pmatrix} r_{MT9,harness} \\ p_{MT9,harness} \\ h_{MT9,harness} \end{pmatrix} - \begin{pmatrix} r_{MT9,0} \\ p_{MT9,0} \\ h_{MT9,0} \end{pmatrix} \right] \right\}. \quad (3)$$

The last two terms of Eqn 3 were used for correction of the misalignment between the optical motion capture and the inertial sensor coordinate system (compare also Eqn 1), and the last three terms eliminated the misalignment between the optical motion capture marker wand and the sensor.

High linear accelerations over a sustained period of time during trot and canter locomotion resulted in a malfunction of the sensor orientation output, which is designed to deal with comparatively low accelerations observed in human locomotion. Therefore, sensor accelerations were low-pass filtered using a 100-sample moving average (effective 3 dB cut-off: 1.1 Hz). The exact realisation of the low-pass filter in this processing step is uncritical, its only purpose being the elimination of acceleration peaks. An additional processing step was required that simulated an initial fixed orientation of the sensor, since capturing was started in full motion of the horse. Five seconds of simulated static data, consisting of sensor acceleration and angular velocity means and magnetometer first frame values, were added to the beginning of the sensor data. These modified data were fed into the sensor orientation algorithm to give the final orientation estimates.

The quality of the orientation output of the inertial sensor was evaluated by means of median and interquartile ranges of the differences between the aligned Euler angles for the two systems.

Linear displacement

The goal was to derive linear displacements in the global coordinate system from the linear accelerations in the sensor coordinate system. This required a projection of the sensor accelerations into the global coordinate system followed by a double integration of the accelerations.

First, the accelerations were projected from the sensor coordinate system into the global system based on the sensor orientation output using the following equation.

$$\mathbf{a}_{global}(t) = \mathbf{R}_{sg}(t)\,\mathbf{a}_{MT9}(t). \quad (4)$$

During the integration process, sensor drift resulted in accumulation of integration errors (Euler integration), and suitable integration constants were required. In the special case of steady-state locomotion, both of these challenges were overcome by assuming cyclical sensor movement. This meant that differences in position (and velocity)

between strides or a series of strides were set to zero. Throughout all experiments, this constraint was implemented by stride-by-stride mean subtraction of x, y and z accelerations and x, y and z velocities using a context window of variable length for calculation of the mean. The results of the integration process are x, y and z displacements in the global coordinate system. The x, y and z displacements derived from the inertial sensor output were compared with those from the optical motion capture system.

The process of integration is summarised in a step-by-step fashion below:

(1) acceleration vectors, $\mathbf{a}_{MT9}(t)$, and Euler angles, $\mathbf{euler}_{MT9}(t)$, acquired from the inertial sensor;

(2) rotation matrix, $\mathbf{R}_{sg}(t)$, calculated at each point in time from corrected Euler angles, $\mathbf{euler}_{MT9,aligned}(t)$, based on Eqn 2;

(3) acceleration vectors, $\mathbf{a}_{MT9}(t)$, projected from the sensor system into the global system using Eqn 4, giving $\mathbf{a}_{global}(t)$;

(4) accelerations cut into stride portions, giving acceleration vectors for each stride i, $\mathbf{a}^i_{global}(t)$;

(5) accelerations mean subtracted using a context window of three strides (one to the left and one to the right) to give $\mathbf{a}^i_{global,meansub}(t)$;

(6) mean-subtracted accelerations integrated to velocities, $\mathbf{v}^i_{global}(t)$, for each stride;

(7) velocities mean subtracted over a context window of three strides [$\mathbf{v}^i_{global,meansub}(t)$];

(8) velocities integrated into displacements $\mathbf{d}^i_{global}(t)$ for each stride.

The implemented mean subtraction using a context window of several strides represents a trade-off between reducing integration errors caused by sensor drift and allowing the integration process to reproduce non-cyclical movements for
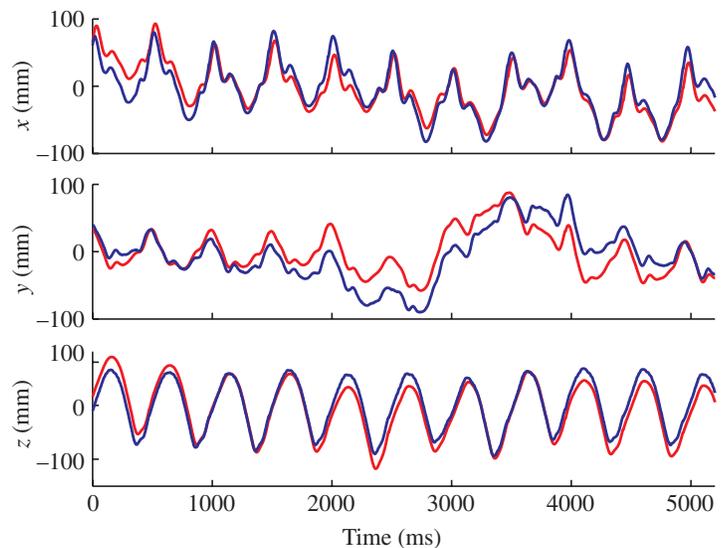

Fig. 4. Displacement data for x (craniocaudal), y (lateral) and z (dorsoventral) movement for optical motion capture (blue) and inertial sensor (red) for a series of strides at canter (9 m s^{-1}). In the integration process, a context window of one stride to each side of the current stride has been used for the mean subtraction.

individual strides. Whereas the use of longer context windows (more strides) will increase drift-related errors, it will enable observation of changes over several strides.

In order to separate slow, non-cyclical components of the linear movements, i.e. those components caused by the subject drifting from side to side over a series of strides, from fast within-stride cyclical components, displacements derived for both inertial sensor and optical motion analysis were high-pass filtered (6th-order Butterworth high pass, 3 dB cut-off at 1 Hz). Since the observed stride frequency values of 1–2 Hz were in the range of this cut-off value, this effectively removed the non-cyclical stride-to-stride differences and allowed us to quantify the ability of the sensor to capture the cyclical components. The individual stride displacement curves were concatenated after the integration, and the entire trace was high-pass filtered. The filtered displacements were then re-segmented into strides and compared in the same way as the unfiltered displacements.

Original and filtered linear displacements derived from the inertial sensor and optical motion capture were compared, and median and interquartile ranges of the differences evaluated.

Experiment 3 – trunk movement of a Thoroughbred horse during treadmill locomotion

The inertial sensor was attached to the horse with the same custom-made harness used in experiment 2 and was used to measure the *x*, *y* and *z* displacements and the roll, pitch and heading angles of the 4th thoracic vertebra while the horse performed a range of speeds and gaits on a high-speed treadmill. The experimental set-up and initial data processing were as described for experiment 2. For each speed increment, inertial sensor data were derived and, in addition to the processing described for experiment 2, data were interpolated to percentage of stride and the mean stride was calculated (six last strides at walk, 12 last strides at trot and 17 last strides at canter). Displacement and orientation amplitudes were calculated.

Results

Experiment 1 – accuracy of optical motion analysis system

The radii of the paths of the two motion analysis markers were 126.1 mm and 127.7 mm, and the mean least-mean-square error calculated over all trials for both markers was 0.58 mm, corresponding to 0.5–3% of the range of motion for the conditions of experiments 2 and 3. Changing the rotation speed of the record player as well as changing the camera positions (around the estimated experimental set-up for experiments 2 and 3) had no measurable effect upon the accuracy with which the system was able to track the 3D position of the two markers and reproduce the circular path.

Experiment 2 – accuracy of MT9 inertial sensor determined by direct comparison with optical motion capture

A total of 35 strides were analysed (6 strides at walk, 12 strides at trot and 17 strides at canter). Displacement data from

the inertial sensor integration process (using a context window of one stride to each side of the current stride) followed the optical motion capture data nicely over a series of strides (Fig. 4). Mean *x*, *y* and *z* displacement and roll, pitch and heading traces obtained using the inertial sensor were virtually indistinguishable from those obtained using optical motion capture (Fig. 5; Table 1). There was, however, a small offset between the inertial sensor and optical motion capture roll and pitch angles. The inertial sensor tended to underestimate the absolute value of roll and overestimate the absolute value of pitch in all gaits, with the magnitude of the offset increasing through the gaits from walk to trot and canter. These errors were gait dependent (Table 1). After high-pass filtering, mean outputs for *x*, *y* and *z* displacements for both methods were still almost identical (Fig. 6; Table 1) and, in addition, decreased standard deviations confirmed the efficacy of the procedure to remove inter-stride differences for both optical motion capture and inertial sensor outputs. Compared with the optical motion capture system, 50% of the values for the *x*, *y* and *z* displacement obtained from the inertial sensor were found within (–1.9, +1.7) mm, (–0.8, +0.9) mm, (–0.6, +0.6) mm for walk, (–2.8, +1.4) mm, (–0.9, +0.9) mm, (–4.3, +4.9) mm for trot and (–3.6, +6.2) mm, (–4, +3.8) mm, (–4.5, +5.1) mm for canter (Table 1). Compared with the range of motion (true values derived from optical motion capture data), these values correspond to a relative error of (–3.3, +3.0)%, (–2.6, +2.9)%, (–2.5, +2.4)% for walk, (–6.5, +3.2)%, (–2.6, +2.6)%, (–5.6, +6.4)% for trot and (–3.2, +5.5)%, (–6.7, +6.3)%, (–3.3, +3.7)% for canter locomotion (Table 1).

The difference (error) between the inertial sensor and the optical motion capture was calculated for each sample across all strides. Error histograms as well as median and interquartile ranges for *x*, *y* and *z* displacements and roll, pitch and heading angles are given to qualitatively and quantitatively demonstrate the ability of the inertial sensor to reproduce the six DoF position of the sensor. For the original data, *x*, *y* and *z* displacements and roll, pitch and heading angles showed error distributions with increasing spread from walk to trot and canter (Fig. 7). With the exception of roll and pitch angles, the errors were distributed around the origin. Roll error data were distributed around median values of 1.4°, 2.6° and 5.4° (with a range of motion of 8.0°, 7.7° and 12.5°), and pitch error data were distributed around median values of –1.0°, –1.7° and –2.4° (with a range of motion of 9.1°, 8.0° and 18.5°) for walk, trot and canter, respectively. After high-pass filtering, the error histograms for linear displacements showed narrower distributions, as confirmed by lower interquartile ranges (Fig. 8; Table 1). Interquartile ranges were reduced by between 14 and 89% by high-pass filtering. For each gait, the highest error reduction was found for the *y* direction, in which the non-cyclical components were most prominent.

Experiment 3 – trunk movement of a Thoroughbred horse during treadmill locomotion

Each variable showed characteristic gait-dependent features (Fig. 5). Whereas walk and trot show typical double-peaked
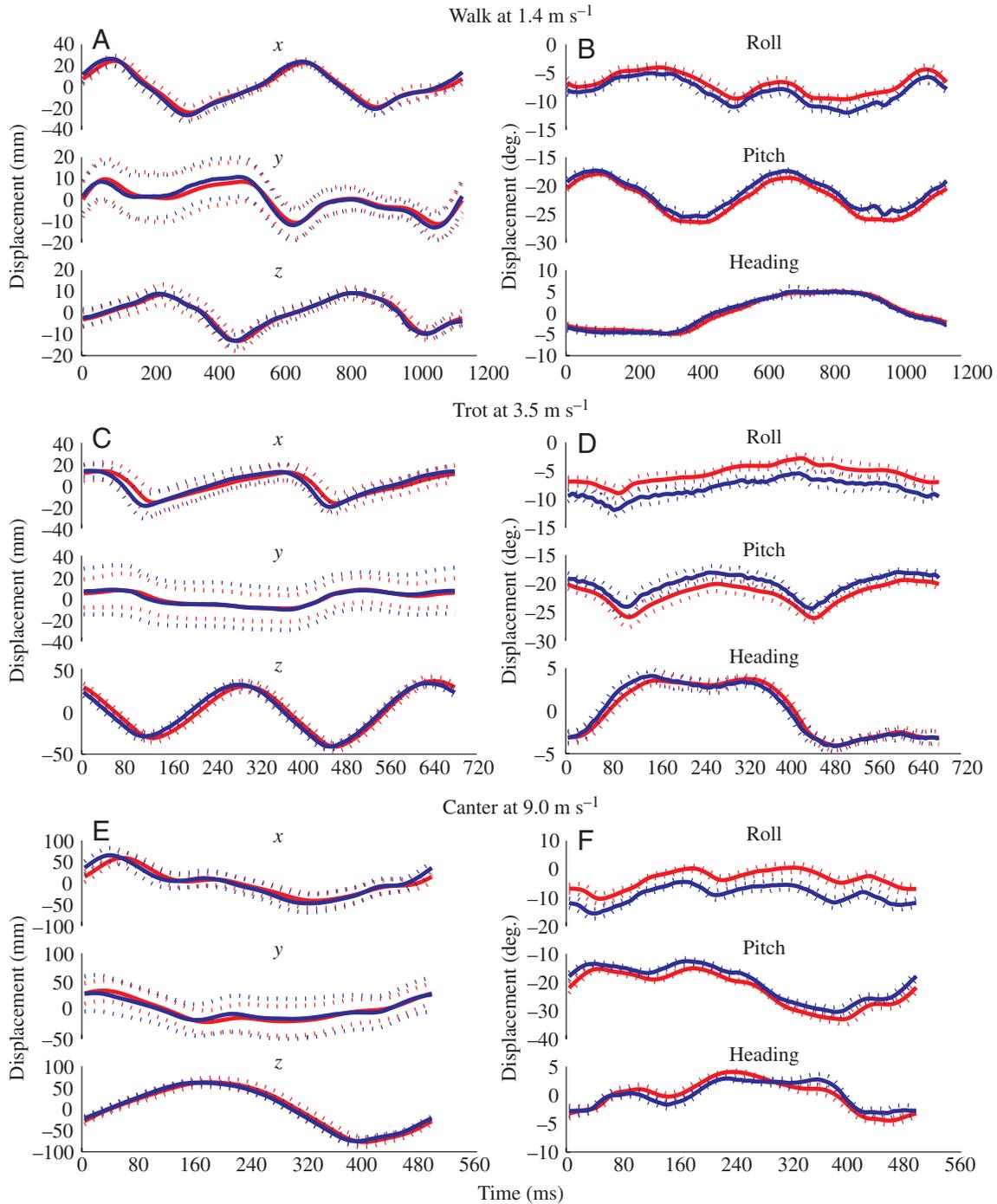
Walk at 1.4 m s⁻¹

Fig. 5. Optical motion capture (blue) and inertial sensor (red) outputs for *x*, *y* and *z* displacements and roll, pitch and heading angles of the sensor mounted over the thoracic spinous processes of a horse during treadmill locomotion (mean ± S.D.). Data are shown for the mean gait cycle (stride) at (A,B) walk (1.4 m s⁻¹), (C,D) trot (3.5 m s⁻¹) and (E,F) left lead canter (9.0 m s⁻¹). For the *x*, *y* and *z* displacements and for the heading angle, the stride-to-stride differences, as indicated by the standard deviations, are bigger than the differences between the two methods (difference between the mean traces). For roll and pitch orientation, however, there is a small offset between the mean traces of the two methods, which increases from walk to trot and canter. The biggest inter-stride variability can be found in the *y* direction for both methods and across all gaits. This demonstrates the tendency of the horse to drift from side to side while performing on the treadmill.

vertical (*z*) displacement curves corresponding to the stance of the left and right leg, the *z* displacement at canter shows a single peak (Minetti et al., 1999).

Ranges of displacement (maximum – minimum value within a stride) for *x*, *y* and *z* displacement were calculated at each speed (Fig. 9). The range of displacement in the *x* (craniocaudal) direction was independent of speed for all gaits. In the *y* (mediolateral) direction, walk showed no speed

Table 1. *Median (med.) and 25th and 75th percentile (25, 75) absolute and relative differences between inertial sensor and motion analysis for* x, y *and* z *displacements*

	Walk				Trot				Canter			
	Med.	25	75	% Red.	Med.	25	75	% Red.	Med.	25	75	% Red.
x in mm (%)												
Original	−0.22 (−0.4)	−2.62 (−4.6)	2.96 (5.2)		1.87 (4.3)	−8.77 (−20.4)	8.23 (19.1)		0.13 (0.1)	−9.69 (−8.5)	10.82 (9.5)	
Filtered	0.44 (0.8)	−1.9 (−3.3)	1.72 (3.0)	35	−1.46 (−3.4)	−2.79 (−6.5)	1.37 (3.2)	76	1.76 (1.5)	−3.64 (−3.2)	6.23 (5.5)	52
y in mm (%)												
Original	2.03 (6.5)	−7.08 (−22.9)	5.94 (19.2)		−1.01 (−3.0)	−8.61 (−25.3)	7.73 (22.7)		−3.82 (−6.4)	−15.47 (−25.8)	13.69 (22.8)	
Filtered	−0.12 (−0.4)	−0.82 (−2.6)	0.90 (2.9)	87	0.03 (0.08)	−0.9 (−2.6)	0.87 (2.6)	89	−0.13 (−0.2)	−3.99 (−6.7)	3.77 (6.3)	73
z in mm (%)												
Original	−0.04 (−0.2)	−2.88 (−12.0)	3.66 (15.3)		0.61 (0.8)	−5.38 (−7.0)	5.33 (6.9)		−0.06 (−0.04)	−6.33 (−4.6)	7.12 (5.2)	
Filtered	0 (0)	−0.6 (−2.5)	0.58 (2.4)	82	−0.27 (−0.4)	−4.31 (−5.6)	4.89 (6.4)	14	−0.7 (−0.5)	−4.54 (−3.3)	5.13 (3.7)	28

Relative errors are given with respect to the true range of motion as derived from optical motion capture data. Data are presented for walk (at 1.4 m s^{-1}), trot (at 3.5 m s^{-1}) and canter (at 9.0 m s^{-1}). Linear displacement differences after high-pass filtering are also given (filtered), and percentage reductions in interquartile ranges after high-pass filtering are shown (% red). This demonstrates the ability to capture the cyclical components of linear movements.

dependence, but amplitude increased with increasing speed at both trot and canter. In the *z* (dorsoventral) direction, only canter showed an effect of speed on amplitude with the range of motion decreasing with increasing speed.

Over the range of speeds and gaits examined here, the observed amplitudes in the *x*, *y* and *z* direction generally agree with previously published values for trunk movement (Buchner et al., 2000). The inertial sensor was mounted over the withers of the horse, which is located at some distance from the CoM, since the position of the CoM is well within the trunk (Buchner et al., 1997). Since rotations of the subject will occur around the CoM, they effectively increase the range of the trunk motion observed by the sensor (Buchner et al., 2000).

Discussion

The inertial sensor proved to be a suitable tool for the tracking of trunk movements. Orientation estimates obtained from the sensor gave median errors for the individual Euler angles in the range of −2.4 to +5.4°. Generally, small errors in absolute orientation have only a minor influence on the projection of linear acceleration into the global coordinate system (and therefore on velocity and displacement). Improvements in gyroscope technology are likely to further reduce the sensor drift and thus increase the accuracy of the orientation estimate. Compared with the range of motion in the *x*, *y* and *z* direction, the sensor error is below 5% for walk and below 7% for trot and canter. Furthermore, the magnetic field sensors, which contribute to the orientation estimation process, are inherently sensitive to distortions of the earth magnetic field, such as those that occur around large metal objects. Since the (mostly metal) treadmill used here weighs 4000 kg, it changes the earth magnetic field, and thus it is likely that the errors reported here are overestimates and that more-accurate orientation data can be expected in experiments under controlled conditions outside the laboratory. On the other hand,

the running of the 15 kW motor of the treadmill did not introduce any changes in orientation output, which is understandable since analogue magnetometer data are low-pass filtered at 10 Hz.

The proposed context-dependent stride-wise mean subtraction process applied to acceleration and velocity represents a trade-off between minimizing integration errors from sensor drift over short time intervals (single strides) and capturing non-cyclical components of movement. A context window of three strides (one to the left and one to the right of the current stride) proved suitable and gave good results for *x*, *y* and *z* displacements in all gaits. In general, smaller context windows resulted in improved cyclical displacement estimates, whereas increasing the context number resulted in overestimations of the non-cyclical parts especially in the *y* direction. This approach to integration is limited as it only resolves for sudden acceleration changes (constant offsets) between strides and thus linear changes in velocity within a stride. This oversimplifies the actual conditions found during animal locomotion. Non-linear, smooth changes of velocity over several strides would represent a better model, but additional knowledge about changes in position and/or velocity over a longer time period would be required to be able to impose more-realistic constraints under these conditions. However, this also means that stride-to-stride changes are small and the context-dependent mean subtraction is a good approximation. The additional information needed for changes in velocity may be derived from further sensors on the subject, such as global positioning system devices (Witte and Wilson, 2004), or from further analysis of the magnetometer signals and might enable us to further enhance the quality of the sensor displacement output. Now global positioning system units with 4 Hz update rate are available, which are especially promising for this. Potentially, changing the configuration of the context-dependent mean subtraction to ignore the current stride will
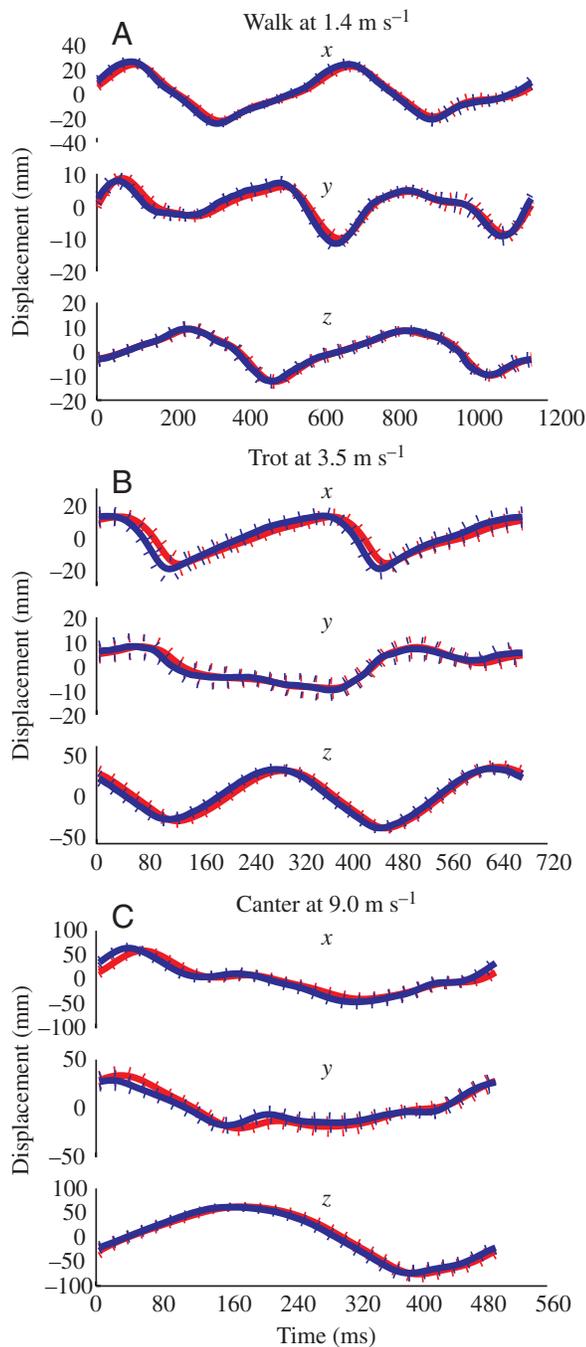
Fig. 6. Motion analysis (blue) and inertial sensor (red) outputs for *x*, *y* and *z* displacements after high-pass filtering (mean ± S.D.). Data are shown for a stride at (A) walk (1.4 m s⁻¹), (B) trot (3.5 m s⁻¹) and (C) left lead canter (9.0 m s⁻¹). Smaller standard deviations (compared with the unfiltered displacements in Fig. 5), especially in the *y* direction, show that high-pass filtering is a valid means of eliminating non-cyclical inter-stride differences of the displacements.

enable us to capture short time deviations from the steady-state pattern.

High-pass filtering proved suitable for separating cyclical and non-cyclical components of the movement across all gaits. At a filter cut-off of 1 Hz, most of the stride-to-stride variations
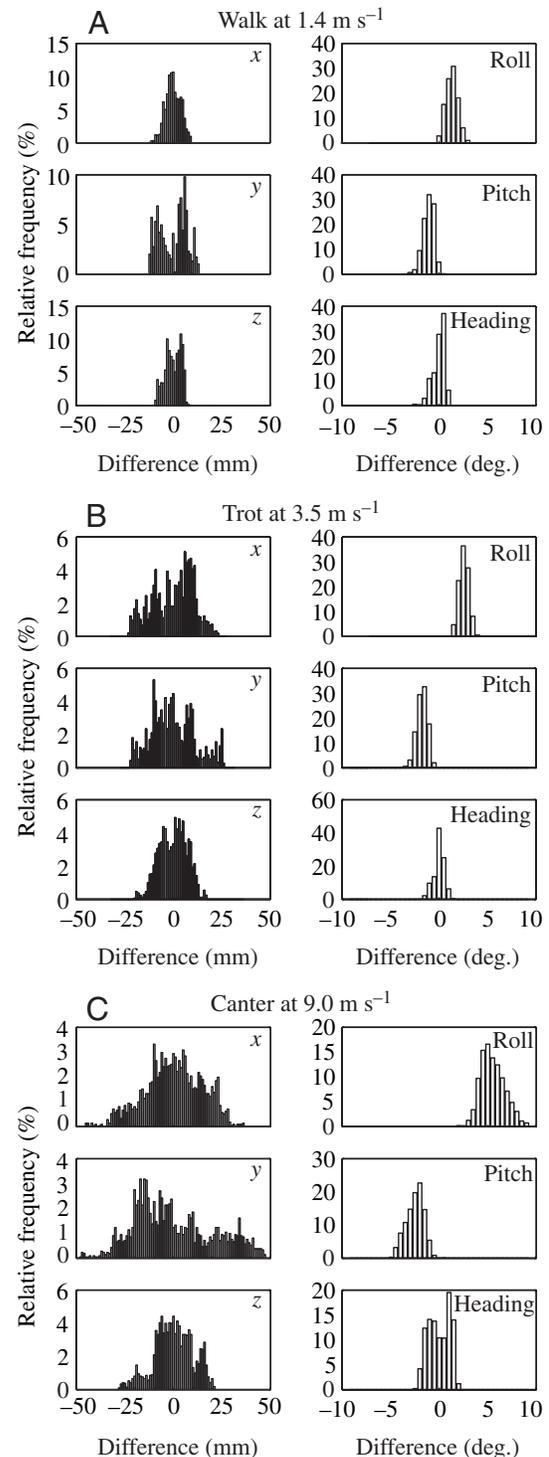

Fig. 7. Histograms of frame-wise difference between motion analysis and inertial sensor for roll, pitch and heading angles and *x*, *y* and *z* displacements for the whole data set. Histograms are shown for (A) walk (1.4 m s⁻¹), (B) trot (3.5 m s⁻¹) and (C) left lead canter (9.0 m s⁻¹). The spread of the histograms is generally increasing from walk to trot and canter. In addition, there is an offset in roll and pitch orientation, which increased with speed.

were eliminated successfully with the biggest improvements found in the *y* direction. This reflects the fact, that the *y*
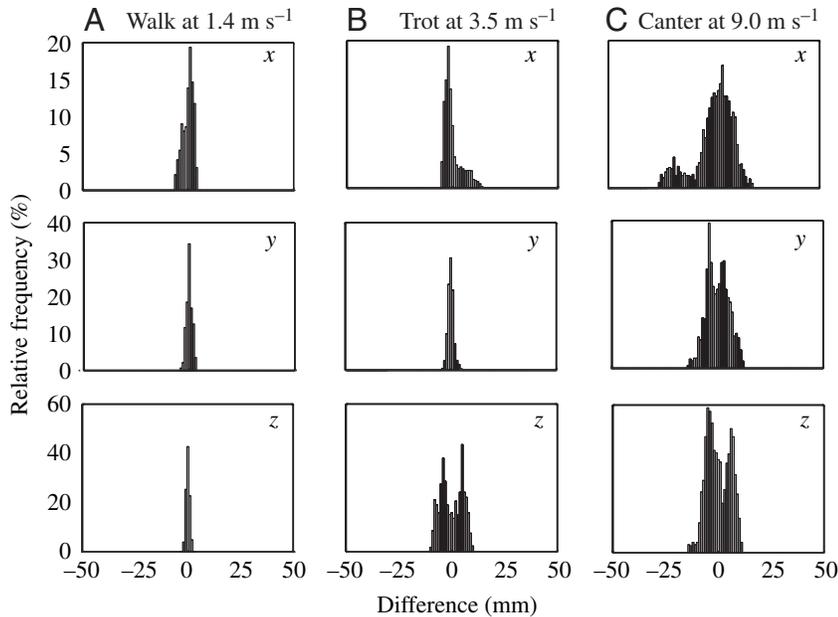
Fig. 8. Histograms of frame-wise difference between motion analysis and inertial sensor *x*, *y* and *z* displacements after high-pass filtering. Histograms are shown for (A) walk (1.4 m s⁻¹), (B) trot (3.5 m s⁻¹) and (C) left lead canter (9.0 m s⁻¹). The reduced spread of the histograms (compared with the unfiltered displacement error histograms in Fig. 7) demonstrates the ability of the inertial sensor integration process to capture the cyclical components of the displacements.

direction, which corresponds to a lateral movement of the horse, showed the highest inter-stride variability before filtering, which is caused by both sudden and gradual lateral drift, i.e. big changes between two strides or a series of small changes for a number of strides. For different applications, a different cut-off frequency might be more suitable. The
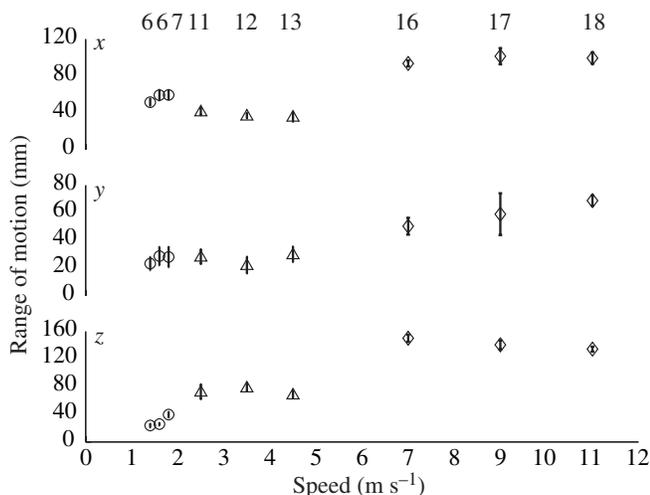

Fig. 9. Ranges of *x*, *y* and *z* displacements are shown as a function of speed and gait for a horse exercising on a treadmill. Ranges are calculated as the difference between maximum and minimum values within the mean stride. Error bars represent ±1 S.D., and the number of strides in each category is given. Walk is represented by open circles, trot by triangles and canter by diamonds.

average improvement over all directions was 68% for walk, 60% for trot and 51% for canter. Although a period of 1 s represented a different number of cycles for each gait (with stride frequencies varying from ~1 Hz for walk to 2 Hz for canter), changing the cut-off frequency to reflect this did not change the results considerably.

Accurate knowledge of the timing of the stride is crucial for the integration process (step 4 in the integration procedure), since a cyclical movement (over a series of strides) is assumed for the mean subtraction. In this study, a limb-mounted accelerometer was used to directly measure the timing of each left front leg footfall. This system is accurate to within 2 ms (less than an inertial sensor sample) across all speeds and gaits on a hard surface (Witte et al., 2004). Errors introduced into the integration can therefore be regarded as negligible. Theoretically, it would be possible to characterise features of the inertial sensor output corresponding to foot placement. However, the indirect and gait-dependent nature of the linkage between the foot and the trunk will inevitably result in reduced accuracy. When possible, the direct method used here is preferable given the importance of appropriate stride segmentation.

The sensor is adequately small and lightweight to be used in field studies (35 g; 39×54×28 mm, width × length × height). Several sensors can easily be mounted on a single subject, allowing relative movements of body segments to be tracked. Since each sensor gives six DoF position information, there is no need to assume rigid links between the segments, and a limited set of sensors is sufficient to capture whole limb movements. However, the experimental conditions have to be evaluated carefully when interpreting the results. The current technique is designed for steady-state movements and gives good results for individual strides (see results without high-pass filtering). In addition, high-pass filtering is an appropriate method for averaging over strides. Whereas experimental set-ups with considerable variations in, for example, slope or surface are still difficult to interpret, field experiments on constant slopes, or comparing different surfaces (with constant or slowly changing surface characteristics), are well within the scope of the technique. In addition, compared with force plate analysis, this technique enables us to capture a series of strides and is cheap in comparison to a multiple-camera motion capture system under field conditions.

In the study described here, data were acquired into a laptop computer alongside the treadmill *via* a serial connection. However, the versatility of the sensor is enhanced because the data stream can be easily logged on the animal into a hand-held computer (depending on the size of the animal) or can be transmitted *via* a high-speed telemetry link to a stationary computer. Links capable of a sufficiently high bandwidth and

range include Bluetooth®, DECT (digital enhanced cordless telecommunications) or wireless networking technology (802.11a-h). When logging is started during locomotion and orientation data are required, the described post-processing step has to be implemented in order to simulate an initial fixed orientation of the sensor. Here, we used a simple moving average filter (effective low pass cut-off of 1.1 Hz) for smoothing the acceleration and gyroscope data. Although the design of this filter is not critical, its only purpose being to simulate fixed orientation (around the mean acceleration), the post-processing step might have to be adapted to the experimental conditions.

Rigid mounting of the sensor on the subject was very important in order to capture accurately overall trunk movement. This was achieved here using the custom-made harness (Fig. 2). There was minimal movement of the sensor relative to the subject, although this was difficult to quantify.

Conclusion

Inertial sensors make it possible to capture cyclical movements with comparable accuracy to optical motion capture systems. This enables the study of (quasi) steady-state field locomotion. The extraction of non-cyclical components of movement is a future goal.

List of symbols and abbreviations

2D	two dimensional
3D	three dimensional
a	acceleration
AD	analogue to digital
CoM	centre of mass
d	displacement
DoF	degree of freedom
E_k	kinetic energy
E_p	potential energy
g	gravity
h	heading
MA	motion analysis
MEMS	micro-electro-mechanical systems
MT9	inertial sensor
p	pitch
r	roll
$\mathbf{R}_{sg}$	rotation matrix sensor to global
v	velocity
x	craniocaudal
y	lateral
z	vertical

References

Barker, R. M. (2004). *Software Support For Metrology Best Practice Guide No. 5, Guide To Eurometros: A Guide For Users, Contributors, And Testers.* Teddington, UK: National Physical Laboratory.

Barrey, E. and Galloux, P. (1997). Analysis of the equine jumping technique by accelerometry. *Equine Vet. J. Suppl.* **23**, 45-49.

Barrey, E., Galloux, P., Valette, J. P., Auvinet, B. and Wolter, R. (1993). Stride characteristics of overground versus treadmill locomotion in the saddle horse. *Acta Anat. (Basel)* **146**, 90-94.

Barrey, E., Evans, S. E., Evans, D. L., Curtis, R. A., Quinton, R. and Rose, R. J. (2001). Locomotion evaluation for racing in thoroughbreds. *Equine Vet. J. Suppl.* **33**, 99-103.

Buchner, H. H., Savelberg, H. H., Schamhardt, H. C., Merkens, H. W. and Barneveld, A. (1994a). Habituation of horses to treadmill locomotion. *Equine Vet. J. Suppl.* **17**, 13-15.

Buchner, H. H., Savelberg, H. H., Schamhardt, H. C., Merkens, H. W. and Barneveld, A. (1994b). Kinematics of treadmill versus overground locomotion in horses. *Vet. Q.* **Suppl. 16, 2**, S87-S90.

Buchner, H. H., Savelberg, H. H., Schamhardt, H. C. and Barneveld, A. (1997). Inertial properties of Dutch Warmblood horses. *J. Biomech.* **30**, 653-658.

Buchner, H. H., Obermuller, S. and Scheidl, M. (2000). Body centre of mass movement in the sound horse. *Vet. J.* **160**, 225-234.

Cavagna, G. A. (1975). Force platforms as ergometers. *J. Appl. Physiol* **39**, 174-179.

Elliott, B. C. and Blanksby, B. A. (1976). A cinematographic analysis of overground and treadmill running by males and females. *Med. Sci. Sport. Exer.* **8**, 84-87.

Ferris, D. P., Louie, M. and Farley, C. T. (1998). Running in the real world: adjusting leg stiffness for different surfaces. *Proc. R. Soc. London Ser. B* **265**, 989-994.

Hedrick, T. L., Usherwood, J. R. and Biewener, A. A. (2004). Wing inertia and whole-body acceleration: an analysis of instantaneous aerodynamic force production in cockatiels (Nymphicus hollandicus) flying across a range of speeds. *J. Exp. Biol.* **207**, 1689-1702.

Leleu, C., Gloria, E., Renault, G. and Barrey, E. (2002). Analysis of trotter gait on the track by accelerometry and image analysis. *Equine Vet. J. Suppl.* **34**, 344-348.

Minetti, A. E., Ardigo, L. P., Reinach, E. and Saibene, F. (1999). The relationship between mechanical work and energy expenditure of locomotion in horses. *J. Exp. Biol.* **202**, 2329-2338.

Nigg, B. M., De Boer, R. W. and Fisher, V. (1995). A kinematic comparison of overground and treadmill running. *Med. Sci. Sport. Exer.* **27**, 98-105.

Skinner, H. B. and Effeney, D. J. (1985). Gait analysis in amputees. *Am. J. Phys. Med.* **64**, 82-89.

Tesio, L., Lanzi, D. and Detrembleur, C. (1998). The 3-D motion of the centre of gravity of the human body during level walking. II. Lower limb amputees. *Clin. Biomech.* **13**, 83-90.

Wilson, A. M., Watson, J. C. and Lichtwark, G. A. (2003). Biomechanics: A catapult action for rapid limb protraction. *Nature* **421**, 35-36.

Witte, T. H. and Wilson, A. M. (2004). Accuracy of non-differential GPS for the determination of speed over ground. *J. Biomech.* **37**, 1891-1898.

Witte, T. H., Knill, K. and Wilson, A. M. (2004). Determination of peak vertical ground reaction force from duty factor in the horse (*Equus caballus*). *J. Exp. Biol.* **207**, 3639-3648.